

Prediction of near-source ground motion exceeding 1g at low frequencies (<2Hz) from Mw~6.5 deterministic physics-based dynamic rupture simulations

L. A. Dalguer

Swiss Seismological Service (SED-ETHZ), Zürich, Switzerland

P. M. Mai

Division of Physical Sciences and Engineering KAUST, Thuwal, 23955-6900, Saudi Arabia



SUMMARY:

Near-source seismic recording of recent earthquakes have revealed that ground motion accelerations exceeding 1g are rather common in moderate shallow earthquakes. Here we use dynamic rupture models to examine PGA-values exceeding 1g at frequencies less than 2Hz in the near-field of moderate earthquakes ($M_w \sim 6.5$). We generate a large number of dynamic source models and evaluate the resulting ground motion. Extreme ground motions appear to be correlated with faulting that breaks the free surface, with largest shaking levels for strike-slip ruptures. For buried ruptures, thrust-faulting earthquakes generate the strongest ground motion, normal faulting the weakest. The predicted near-source acceleration ground motion of dipping faults shows asymmetry in the acceleration time history. This asymmetry in our numerical simulation is pronounced in the vertical and normal components and is attributed to the source effect due to the Kostrov-like slip velocity characteristics that dominates the near source ground motion.

Keywords: extreme ground motion, near-source ground motion modelling, rupture dynamic

1. INTRODUCTION

Modern dense near-source seismic recording of recent earthquakes have revealed that ground motion accelerations exceeding 1g are rather common in moderate shallow earthquakes (e.g. 2008 M_w 6.9 Iwate-Miyagi Nairiku, Japan; 2010 M_w 7.0 Darfield, New Zealand; 2011 M_w 6.3 Christchurch, New Zealand) in the frequency range of engineering interest (< 10.0 Hz). Recorded peak accelerations above 1g at relatively low frequency of ~ 1.0 Hz during the 2011 M_w 6.3 Christchurch event are particularly surprising, and can be extremely damaging for tall buildings.

Earthquake numerical models based on physics of the causative rupture and wave propagation that incorporate conservation laws of continuum mechanics, frictional sliding, and the state of stress in the crust, have expanded our understanding of both source- and propagation-dominated ground motion phenomena (e.g., Dunham and Archuleta, 2005; Dalguer et al, 2008; Olsen et al, 2009). In these models the fault kinematics (slip and slip rate) and rupture propagation are determined dynamically as part of the solution of the problem by solving the elastodynamic equation coupled to frictional sliding. They usually idealize the earthquake rupture as a propagating shear crack on a frictional interface embedded in a linearly elastic continuum. This idealization has proven to be a useful foundation for analyzing and simulating natural earthquakes (e.g., Andrews, 1976; Day, 1982; Olsen et al., 1997; Oglesby et al., 1998; Dalguer et al., 2001; Day et al., 2008, Oglesby and Mai, 2012), and we adopt it here. The use of dynamic rupture models to simulate earthquakes is gaining increasing importance in the Earth science and earthquake engineering community, as these models more accurately incorporate the physical processes of earthquakes and thus have greater potential to capture details of the physical rupture process and near-source ground motion variability. Understanding these aspects improve our

capability to predict near-source ground motion, and therefore allows a more accurate assessment of the seismic hazard and risk.

Here we use dynamic rupture models, using the Support Operator Rupture Dynamics code (SORD) of Ely et al., 2009, to examine PGA-values exceeding 1g at frequencies less than 2Hz in the near-field of moderate earthquakes ($M_w \sim 6.5$). We generate a large number of dynamic source models (Dalguer and Mai, 2011) and evaluate the resulting ground motion characteristics for three classes of faulting (thrust, normal and strike slip) for buried and surface-rupturing earthquakes. Stress and frictional strength are modeled using two end-member cases of normal stress: 1) depth-dependent; and 2) depth-independent normal stress. Our simulations are tailored to create a set of 30 $M_w \sim 6.5$ scenario earthquakes for each faulting style and each normal-stress parameterization (buried and surface faulting with depth and non-depth normal stress dependent), leading to a total of 360 simulations. The resulting ground motions are compared to empirical ground motion predictions equations (GMPE's). Models predicting acceleration exceeding 1g are evaluated with appropriate recent near-field observations. This diversity of rupture models generates a broad range of scenarios for also evaluating near-source ground motion variability, and for identifying the causes for extreme ground motion.

2. DYNAMIC RUPTURE MODEL

Assuming that shear failure on pre-existing faults of shallow earthquakes is governed by Coulomb friction, the mode of faulting and the loading history in compressional and extensional tectonic regimes play an important role in determining the initial stress and the absolute value of frictional strength on the fault (e.g. Sibson, 1991). Considering a fault system under confining pressure equivalent to the gravitational load, the tectonic loading in a compressional regime accumulates shear stress on the fault while simultaneously frictional strength is expected to increase due to increasing normal stress. In contrast, tectonic loading in an extensional regime results in a reduction of the shear strength due to decreasing normal stress.

2.1 Normal Stress Depth Dependent Model.

Our chosen stress parameterizations follow the methodology proposed by Dalguer and Mai (2008) to estimate the strength and initial stress on the fault prior to rupture. This approach combines stochastic initial stress fields with a realistic fault-loading environment in which the tectonic loading regime (compressional or extensional) and the gravitational loading determine the absolute value of fault frictional resistance and initial stress. The procedure is as follows:

1) Assumption on far-field stress: Initially, the far-field stresses are equal to the confining pressure which in turn is equivalent to the gravitational load

$$\sigma_1 = \sigma_2 = \sigma_3 = \rho gh \quad (2.1)$$

where σ_1 , σ_2 and σ_3 are the principal stresses, ρ the density, g the acceleration of gravity, and h the depth.

2) Fault loading: Adjust principal stresses according to faulting regime, i.e. increase σ_1 for thrust or strike-slip faulting, decrease σ_3 for normal faulting events. This represents a “loading” or stress-increasing mechanism for thrust/strike-slip events, and an “unloading” or stress-reduction mechanism for normal faults.

$$\begin{aligned}\sigma_1 &= \rho gh + \Delta\sigma_{load} && \text{loading} \\ \sigma_3 &= \rho gh + \Delta\sigma_{load} && \text{unloading}\end{aligned}\tag{2.2}$$

where $\Delta\sigma_{load}$ is the stress increment/decrement to load/unload the system

3) Fault-normal stress: Estimate the normal stress acting on a specific fault plane from the loaded/unloaded principal stresses, using

$$\sigma_n = \frac{1}{2}(\sigma_1 + \sigma_3) + \frac{1}{2}(\sigma_1 - \sigma_3)\cos(\theta)\tag{2.3}$$

where θ is the fault plane angle measured with the σ_3 axes .

4) Fault friction: Estimate the frictional strength (assuming Coulomb friction) on the fault, based on

$$\tau_c = c + \mu_f(\sigma_n - p)\tag{2.4}$$

where c is cohesion stress, and p is pore pressure (here: hydrostatic pressure); the effective normal stress is then given by $(\sigma-p)$; μ_f is the friction coefficient that depends on slip (slip weakening model) in the form given by Andrews (1976) as follow

$$\mu_f = \begin{cases} \mu_s - (\mu_s - \mu_d)u / d_0 & u < d_0 \\ \mu_d & u \geq d_0 \end{cases}\tag{2.5}$$

where μ_s and μ_d are respectively the static and dynamic friction coefficient, u the slip and d_0 the critical slip distance.

5) On-fault shear stress: In our approach, the initial shear stress on the fault is then given by

$$\tau_0 = \tau_{st} + \Delta\tau_{ld}\tag{2.6}$$

where τ_{st} is a heterogeneous stress field (Ripperger et al., 2007, 2008) generated as a spatial random field that represents the remaining stress from the history of previous events. This stochastic stress is first tapered in an arbitrary non-depth dependent frictional strength profile such that its maximum (τ_{max}) is close to the static failure stress (τ_s) and its minimum (τ_{min}) is the final stress from the last past earthquake characterized with the dynamic overshoot ($k_{osd} > 1$) or undershoot ($k_{osd} < 1$) coefficient.

$$\tau_{max} = \tau_s; \quad \tau_{min} = \tau_s - (\tau_s - \tau_d)k_{osd}\tag{2.7}$$

Finally, the τ_{st} is again tapered to the depth dependent frictional strength profile calculated in Step 4, but keeping the same ratio $(\tau_0 - \tau_d)/(\tau_s - \tau_d)$, where τ_s and τ_d are respectively the static and dynamic frictional strength. $\Delta\tau_{ld}$ in Equation 2.6 is a small stress increment for additional loading in the nucleation zone in order to initiate rupture instability (Ripperger et al 2007, 2008).

6) Nucleation zone: Determine the size of the nucleation zone, a circular patch with radius L_c , half of the critical length of an equivalent uniform fault with initial stress and frictional strength corresponding to the average over the fault. L_c has the form (e.g, Day et al, 2005):

$$L_c = \frac{\mu d_0 (\tau_{bav})}{\pi (\Delta \tau_{av})^2} \quad (2.8)$$

where μ is the shear modulus and τ_{bav} and $\Delta \tau_{av}$ are respectively the average breakdown strength drop and average stress drop. Depending on the stress parameterization, L_c may take on large values. Because large nucleation regions would influence the dynamic rupture properties over a large fault area, it is necessary to choose L_c as small as possible. Our numerical experiment shows that with $L_c = 2.0$ km is often enough to trigger rupture, so we assumed a maximum L_c of 2.0 km. The center of the nucleation zone is given stochastically, defined as the point in which the initial stress is equal to the yielding stress, as defined in step (5).

7) Depth-dependent crustal strength: As shown in Figure 1, our parameterization considers a stable zone (shallow part), a brittle crust (seismogenic zone) and a ductile zone (deepest layer). The parameterization with depth-dependent normal stress produces a weak zone at shallow depth incapable of maintaining large shear stress. If this shallow depth is parameterized inappropriately, early and unrealistic rupture process may take place in this zone. In addition, previous works (e.g. Brune and Anooshehpour, 1998; Day and Ely, 2002) suggest that rupture within this weak shallow zone should operate in a distinctively different fashion than the rest of the fault, i.e. showing strength hardening due to the formation of incompetent fault gouge, micro cracking (e.g. Marone, 1998; Marone and Scholz, 1988), or fissuring of rocks and other forms of off-fault zone damage due to the presence of sedimentary surface deposits. The main feature of this shallow depth zone is that it operates during rupture with an enhanced energy absorption mechanism. We therefore define the first 2 km depth as a weak shallow zone that follows strength hardening during frictional sliding. To model this frictional behavior, we assume negative stress drop and large critical slip distance in the stable uppermost layer (Figure 2.1). The seismogenic zone, below the stable zone, represents the brittle crust of the earth. We model it as an 18 km thick layer. Below this seismogenic layer, we consider a ductile zone, characterized by large critical slip distance (Figure 2.1). Rupture may propagate dynamically into the weak shallow layer or into the deep ductile zone, but cannot nucleate in this region. Once the dynamic rupture has entered this zone, it quickly terminates as the energy-absorption at the crack tip exceeds the energy supplied by the propagating crack.

2.2 Normal Stress Non-depth Dependent Model.

The stress parameterization for this case follows the same procedure as described above, with the difference that the normal stress acting on the fault is constant over the fault.

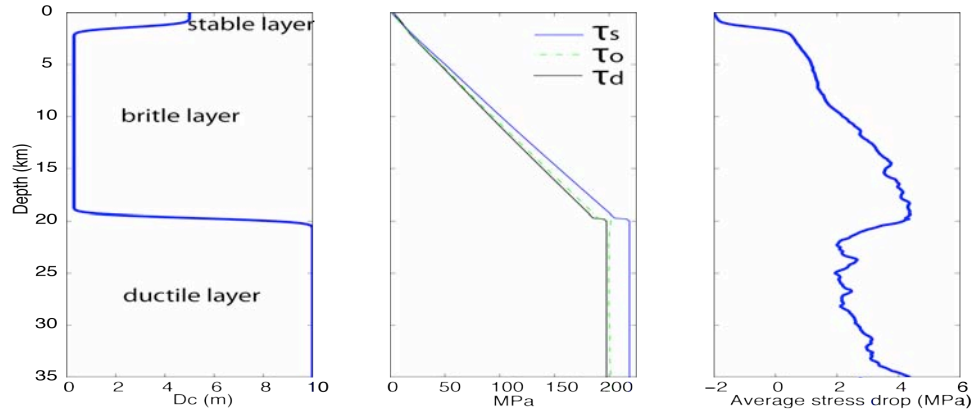


Figure 2.1. An example of depth variation of frictional parameters averaged along the strike of the fault, adopted in the dynamic rupture models. Left figure shows critical slip distance. Center shows the static frictional strength (τ_s), initial stress (τ_o) and dynamic frictional strength (τ_d). Right figure shows the stress drop.

2.3 Model Parameterization

The list below summarizes the modeling parameters adopted in our dynamic rupture simulations:

- Strike-slip faulting: dip=90° fault length = 30km fault width=12km
- Thrust faulting: dip=45° fault length = 24km fault width=15km
- Normal faulting dip=60° fault length = 24km fault width=15km
- For ruptures that are not allowed to break the surface, the faults are buried at 5km depth
- Static friction coefficient = 0.6 dynamic friction coefficient = 0.56 cohesion force = 1.0×10^6 Pa;
- dynamic overshoot coefficient = 1.5 critical slip distance = 0.2
- critical slip distance smoothly increases from 0.3 m to 5 m at fault boundaries in a 3 km-wide buffer zone that surrounds the above defined fault areas; this approach ensures that rupture propagation stops smoothly at the borders of the fault
- loading under compression (trust/ strike slip fault), unloading under extension (normal fault) = 50×10^6 Pa. The loading is applied at 15km depth.
- strike-slip faults have the principal stress σ_2 equal to the average between σ_1 and σ_3 , and the angle θ of equation 2 is 45° (fault plane angle measured with the σ_3 axes)
- initial stress stochastic field realizations based on von Karman distribution with correlation length of 8.0 km in along-strike and along-dip direction, Hurst number $H = [0, 0.25, 0.5]$; resulting stress distribution are hence compatible to seismological observations (Mai and Beroza, 2002).
- normal stress = 120 MPa, for model with non-depth dependent stress
- layered 1D velocity-density structure, derived as the average model of available models in Switzerland (Figure 2.2)
- numerical setup uses 8 grid element per wavelength; a conservative estimate yields that we accurately resolve a maximum frequency of ~ 3 Hz, given the chosen velocity structure and grid size of 100 m; domain-size 100 km x 100 km x 30 km
- simulations were carried out on a Cray XT5 at the Swiss National Supercomputing Center (CSCS) on 4096 CPUs; a typical run requires about 1hr, i.e. we used ~ 4000 CPU-hrs per simulation.

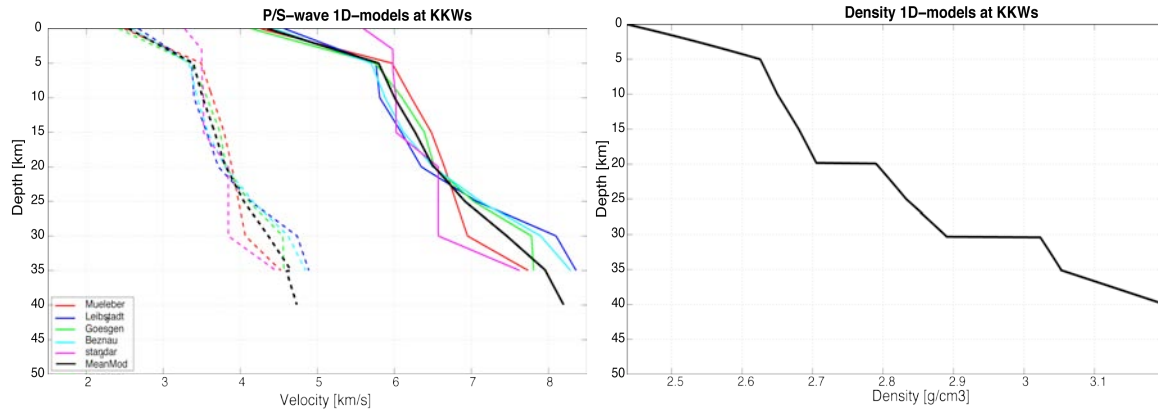


Figure 2.2 1D velocity structure model (left) and density (right) used for dynamic rupture simulations.

3. NUMERICAL RESULTS

From the total of 360 models that include buried and surface ruptures, with both constant and depth-dependent normal stress depth, for three classes of faulting (strike, reverse and normal-slip), a diversity of rupture scenarios has been simulated in a range of M_w 5.5 – 7.0. Figure 3.1 shows the dynamic rupture solution (slip, peak slip rate, rupture time and stress drop distribution) of a representative model of normal faulting M_w 6.55.

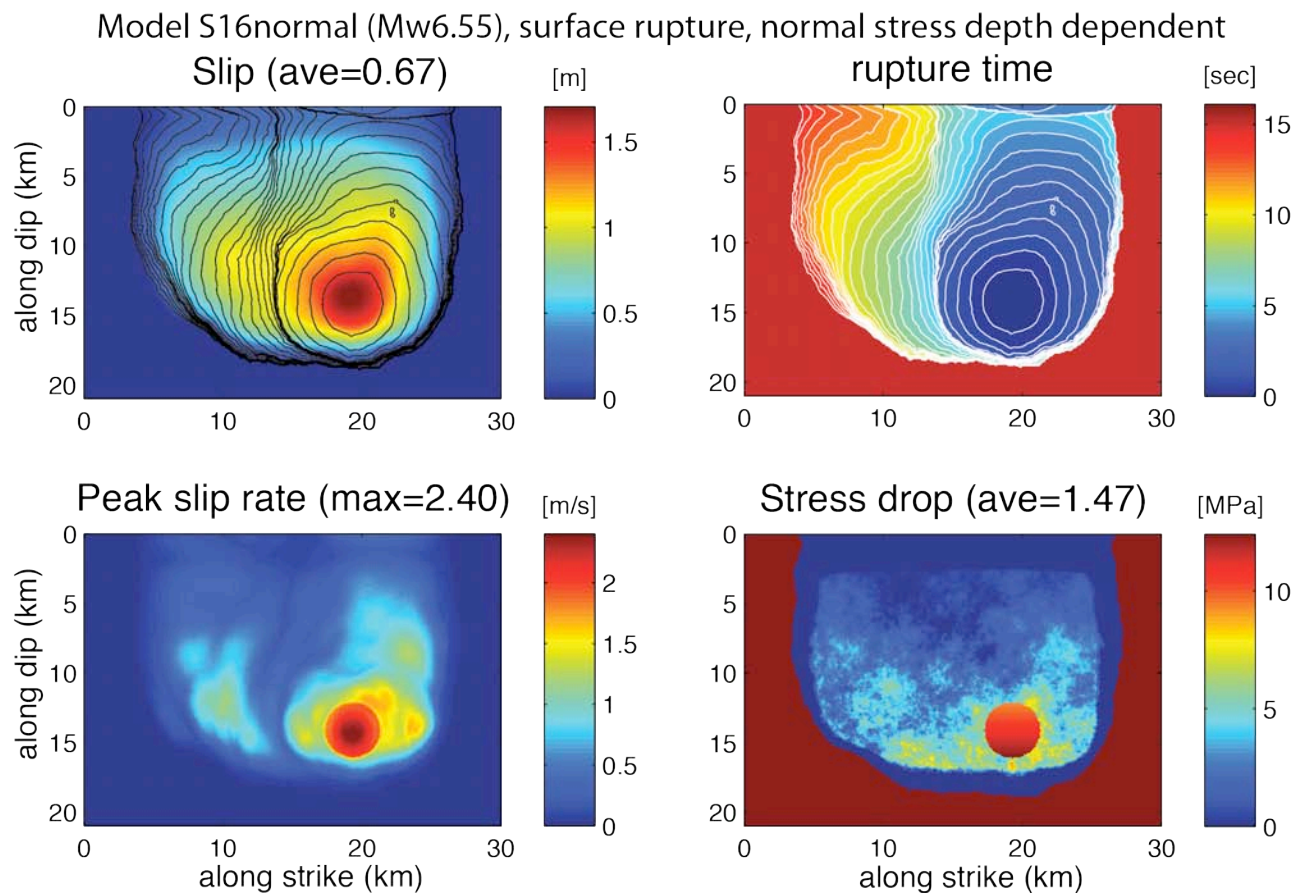


Figure 3.1. Dynamic rupture solutions for the surface rupturing model “s16normal”. Top left shows slip distribution (contour line is the rupture time each 0.5 sec); top right is image map and contour line of rupture time; bottom left is peak slip rate; and bottom right is the stress drop distribution.

From the dynamic rupture simulations we save the resulting near-source ground-motions at 168 locations around the fault, arranged in a race-track pattern with distances out to ~ 50 km from the surface projection of the top of the fault plane. Figure 3.2 shows the PSA for period of 1.0s of the set of 360 rupture models compared with the GMPE's from Akkar and Bommer (2010) denoted as AK10 and Boore and Atkinson (2008) denoted as BA08, for $V_{s30}=1500\text{m/s}$. Site-amplification corrections using the period-dependent amplification coefficient of Borchardt (1994, 2002) are applied to scale computed ground motions to $V_{s30}=1500\text{m/s}$ from the minimum shear-wave velocity in our simulations ($V_{s30}=2500\text{m/s}$). This correction is needed to facilitate the comparison with the GMPE's that are based on V_{s30} -values less than 1500 m/s. Synthetic ground motions are filtered using a band pass Butterworth filter from 0.01 to 3.0 Hz. In general, the simulated PSA are consistent with the GMPE's, with better fitting at distance R_{jb} larger than about 3-7 km than at very close distances to the fault. Estimates using the maximum ground-motion value from the two horizontal components provide a somewhat better agreement with the GMPE's than the geometric mean of the horizontal components. Most importantly, we find an increased variability in the near-field of the rupture; the typical near-source saturation of GMPE-predicted ground-motions is not obvious in our calculations. Rather, there are significant ground-motion reductions near the source for buried faults and for dip-slip ruptures, but considerable increase for strike slip surface rupturing earthquakes.

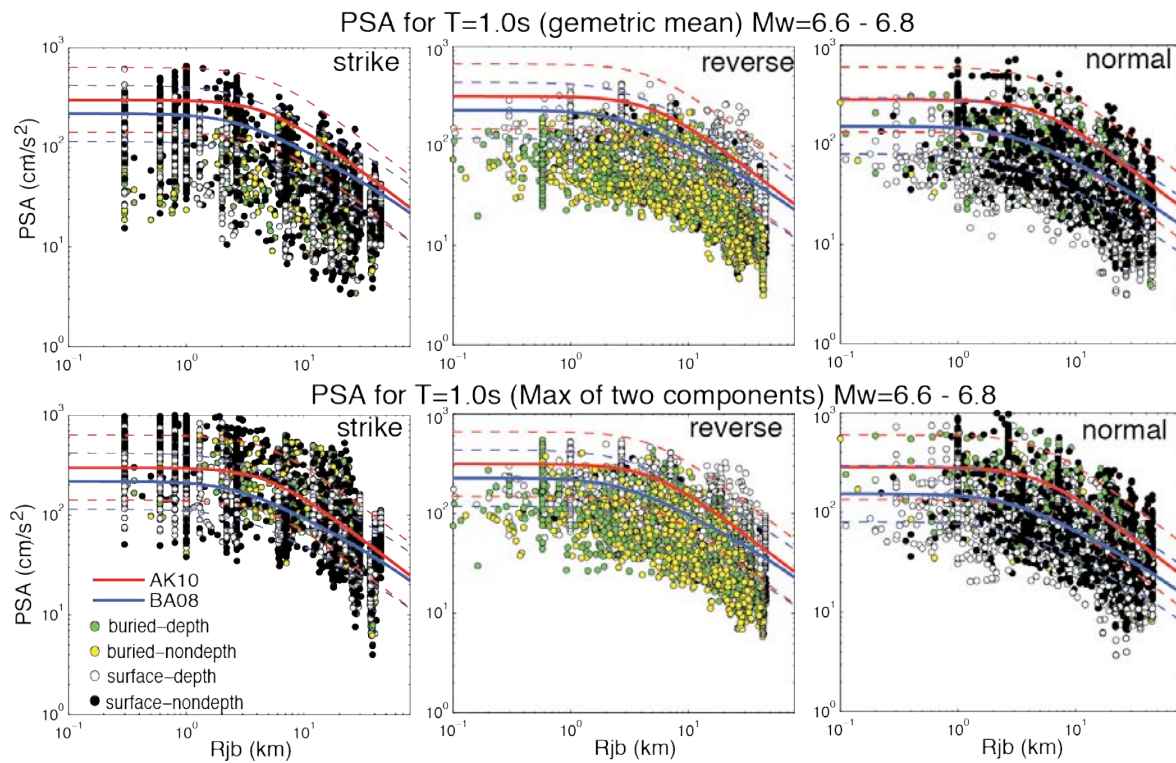


Figure 3.2. Horizontal Pseudo Spectral Acceleration (PSA) for $T=1.0\text{s}$, compared to GMPE AK10 (Akkar and Bommer, 2010) and BA08 (Boore and Atkinson, 2008) for strike-slip, reverse and normal faults of buried and surface rupturing events with depth and non-depth dependent stress (magnitude range M_w 6.6 – 6.8). Top: comparison using the geometric mean; bottom :comparison with maximum of the two horizontal components.

Figure 3.3 displays PGV and PGA ($f_{\text{max}} = 3$ Hz) for all the 360 rupture models. We find that surface rupturing models predict stronger ground motion than buried rupture, with the strongest shaking occurring for non-depth dependent stress models and accelerations exceeding in some case gravity. Strike slip models predict the strongest ground motion, followed by reverse-slip rupture models.

Maximum ground motion levels is constant up to $M_w \sim 6.3$ for strike slip fault, and up to $M_w \sim 6.7$ for reverse and normal faults. Differences in ground-motions between buried ruptures with depth and non-depth dependent stress are indistinguishable.

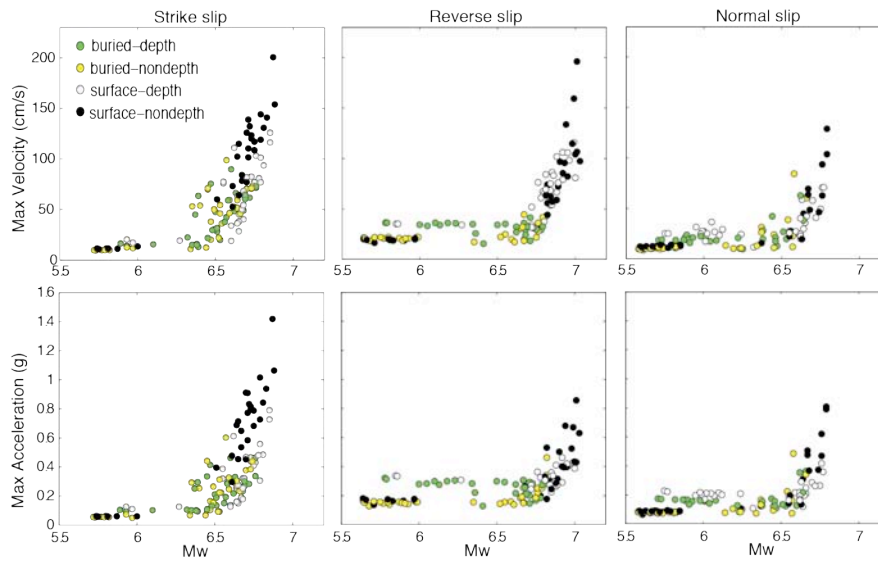


Figure 3.3. Maximum horizontal ground motion for 360 events for strike-slip, reverse and normal faulting (buried and surface rupturing; depth and non-depth dependent stress) for a total of 360 models. Top: velocity; bottom: acceleration

Extreme ground motion appear to be correlated with faulting that breaks the free-surface, with the strongest shaking occurring for strike-slip rupture for which ground accelerations may exceed gravity. Figure 3.4a shows a representative PSA exceeding the gravity predicted by surface rupturing of strike, reverse and normal-faulting models with non-depth dependent normal stress. As seen in this figure, gravity is exceeded at frequencies in the range of 1.0 – 2.5 Hz ($T = 0.4 – 1.0$ s). For reference, Figure 3.4b displays PSA at several stations exceeding gravity during the 2011 M_w 6.3 Christchurch, New Zealand earthquake, in which extreme ground motion were observed in the same frequency range.

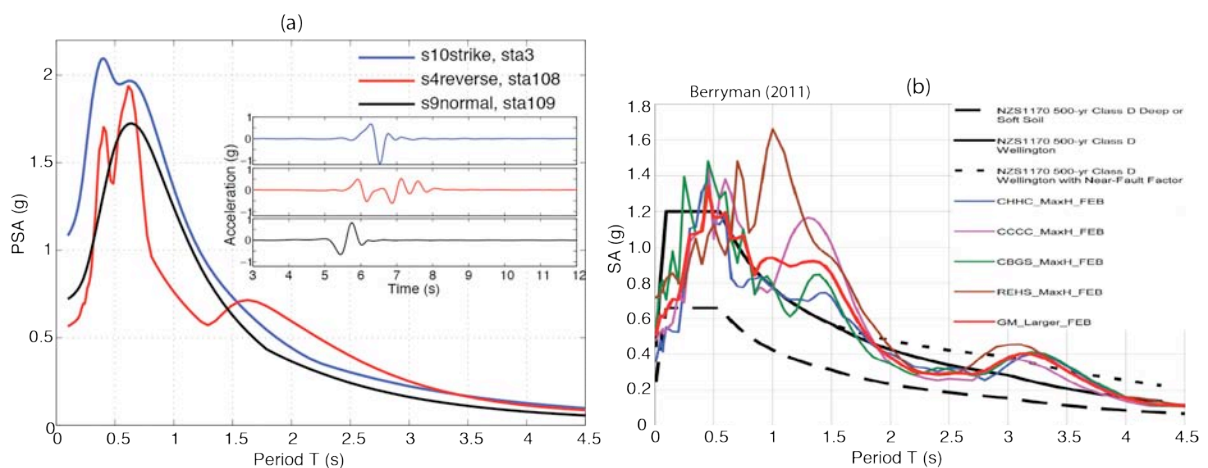


Figure 3.4. Left (a) PSA at selected station near the source for strike, reverse and normal faulting with surface rupturing and non-depth dependent stress; the inset figure displays the corresponding acceleration time histories. Right (b), Spectral Acceleration at several stations exceeding gravity during the 2011 M_w 6.3 Christchurch, New Zealand earthquake (After Berryman, 2011). Solid and dashed black line are design spectral motions.

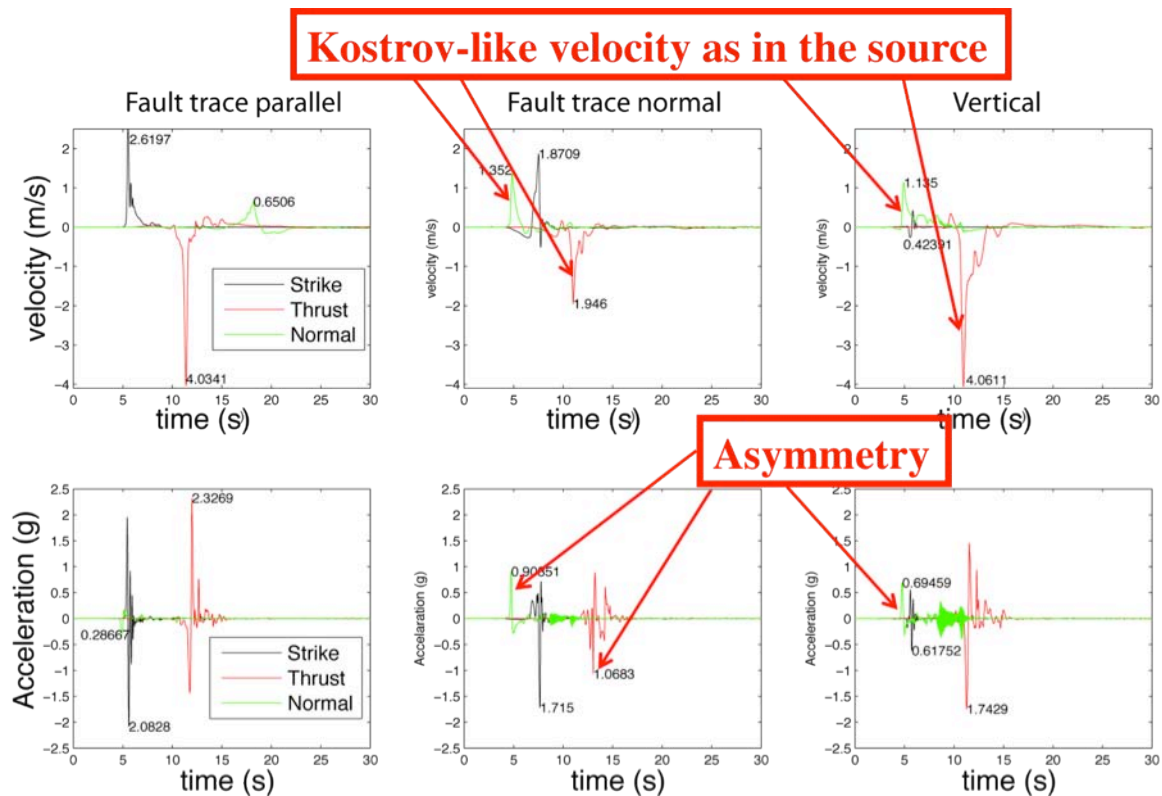


Figure 3.5. Near-field velocity (top) and acceleration (bottom) waveforms for surface-breaking strike-slip, thrust and normal faulting. Red arrows point Kostrov-like velocity ground motion (top) and asymmetric acceleration ground motion (bottom).

Figure 3.5 displays near-source velocity and acceleration waveforms, showing asymmetry in the acceleration time history as expected for dipping faults. The asymmetry seen in our numerical simulation is also pronounced in the vertical and normal components, and can be attributed to source effect due to the Kostrov-like slip velocity characteristics that dominates the near source ground motion. Notice that the normal component for strike slip fault also generate asymmetric ground motion acceleration. For accelerations above 1g this asymmetry is more noticeable in observed natural earthquakes (e.g. Aoi et al, 2008; Yamada et al, 2009).

4. CONCLUSIONS

Our suite of rupture dynamic simulation shows that extreme ground motions appear to be correlated with faulting that breaks the free surface, with largest shaking levels for strike-slip ruptures. For buried ruptures, thrust-faulting earthquakes generate the strongest ground motion, normal faulting the weakest. In general, simulated ground motion are consistent with GMPE's at distance $>5\text{km}$, but not at short distance. The predicted near-source acceleration ground motion of dipping faults shows asymmetry in the acceleration time history. The asymmetry in our numerical simulation is pronounced in the vertical and normal components, and arises due to the near-field Kostrov-like slip velocity characteristics that dominates the near source ground motion. For accelerations above 1g this mentioned asymmetry is more noticeable in observed natural earthquakes.

ACKNOWLEDGEMENT

Numerical simulations were done at the Swiss National Supercomputing Center (CSCS), under the production project "Development of Dynamic Rupture Models to Study the Physics of Earthquakes and Near-Source Ground Motion".

REFERENCES

- Akkar, S. and J. J. Bommer (2010), "Empirical Equations for the Prediction of PGA, PGV and Spectral Accelerations in Europe, the Mediterranean Region and the Middle East", *Seismol. Res. Lett.*, Vol. 81, No. 2, pp. 195-206.
- Andrews, D.J (1976). Rupture velocity of plane-strain shear cracks, *J. Geophys. Res.*, 81, 5679-5687.
- Aoi, S.; T. Kunugi and H. Fujiwara (2008). Trampoline Effect in Extreme Ground Motion, *Science* 322, 727, DOI: 10.1126/science.1163113.
- Berryman, K (2011), A tale of two earthquakes – the Christchurch sequence of 2010-2011, Proc. G-Event1 Conference, Tsukuba, march 2011.
- Boore, D. M., and G. M. Atkinson (2008), "Ground-motion prediction equations for the average horizontal component of PGA, PGV, and 5%-damped PSA at spectral periods between 0.01 s and 10.0 s", *Earthq. Spectra*, Vol. 24, No. 1, pp. 99-138.
- Borcherdt RD (1994) Estimates of site-dependent response spectra for design (methodology and justification). *Earthquake Spectra* 10(4):617–653.
- Borcherdt RD (2002) Empirical evidence for acceleration-dependent amplification factors. *Bull. Seis Soc Am.* 92(2):761–782
- Dalguer L.A. and P. M. Mai (2011), Near- Source Ground Motion Variability from M~6.5 Dynamic Rupture Simulations. 4th IASPEI / IAEE International Symposium: Effects of Surface Geology on Seismic Motion, In CD. August 23–26, 2011, University of California Santa Barbara, CA, USA.
- Dalguer L.A; Irikura K; Riera J. And Chiu H.C (2001). The Importance of the Dynamic Source Effects on Strong Ground Motion During the 1999 Chi-Chi (Taiwan) Earthquake: Brief Interpretation of the Damage Distribution on Buildings. *Bull. Seismol. Soc. Am.*, 95, 1112-1127.
- Dalguer, L. A. and Day, S. M. (2007), Staggered-Grid Split-Nodes Method for Spontaneous Rupture Simulation. *J. Geophys. Res.*, 112, B02302, doi:10.1029/2006JB004467.
- Dalguer, L.A., H. Miyake, S.M. Day and K. Irikura (2008), Surface Rupturing and Buried Dynamic Rupture Models Calibrated with Statistical Observations of Past Earthquakes. *Bull. Seismol. Soc. Am.* 98, 1147-1161, doi: 10.1785/0120070134.
- Dalguer, L.A. and M. Mai (2008), Implications of Style-of-Faulting and Loading Characteristics on the Dynamic Rupture Process, *Eos Trans. AGU*, 89(53), Fall Meet. Suppl., Abstract S51D-1798
- Day, S. M. (1982). Three-dimensional simulation of spontaneous rupture: the effect of nonuniform prestress, *Bull. Seismol. Soc. Am.*, 72, 1881-1902.
- Day, S. M., L. A. Dalguer, N. Lapusta, and Y. Liu (2005), Comparison of finite difference and boundary integral solutions to three-dimensional spontaneous rupture, *J. Geophys. Res.*, 110, B12307, doi:10.1029/2005JB003813.
- Day, S. M., S. H. Gonzalez, R. Anooshehpour, and J. N. Brune (2008). Scale-model and numerical simulations of near-fault seismic directivity, *Bull. Seism. Soc. Am.* , Vol. 98, doi: 10.1785/0120070190, pp. 1186-1206
- Dunham, E., and R. Archuleta (2005). Near-source ground motion from steady state dynamic rupture pulses, *Geophys. Res. Lett.* 32, L03302, doi:10.1029/2004GL021793.
- Ely, G., S.M. Day, and J-B. Minster (2009). Dynamic rupture models for the southern San Andreas fault, *Bull. Seism. Soc. Am.*, 100 (1), 131-150, doi:10.1785/0120090187.
- Mai, P.M., and G.C. Beroza (2002). A spatial random-field model to characterize complexity in earthquake slip, *J. Geophys. Res.*, 107(B11), 2308, doi:10.1029/2001JB000588, 2002.
- Oglesby, D. and P.M. Mai (2012) Fault geometry, rupture dynamics and ground motion from potential earthquakes on the North Anatolian Fault under the Sea of Marmara, *Geophys. J. Int.*, doi: 10.1111/j.1365-246X.2011.05289.x.
- Olsen, K. B., R. Madariaga, and R. Archuleta (1997). Three Dimensional Dynamic Simulation of the 1992 Landers Earthquake, *Science*. 278, 834-838.
- Olsen, K., S.M. Day, L.A. Dalguer, J. Mayhew, Y. Cui, J. Zhu, V.M. Cruz-Atienza, D. Roten, P. Maechling, T.H. Jordan, D. Okaya and A. Chourasia (2009) ShakeOut-D: Ground motion estimates using an ensemble of large earthquakes on the southern San Andreas fault with spontaneous rupture propagation, *Geophys. Res. Lett.*, 36, L04303, doi:10.1029/2008GL036832.
- Ripperger, J., J. P. Ampuero, P.M. Mai, and D. Giardini (2007). Earthquake source characteristics from dynamic rupture with constrained stochastic fault stress, *J. Geophys. Res.* 112: B04311, doi:10.1029/2006JB004515.
- Ripperger, J.; P. M. Mai and J.-P. Ampuero (2008) Variability of near-field ground motion from dynamic earthquake rupture simulations *Bull. Seism. Soc. Am.*, 98 (3), 1207-1228; doi:10.1785/0120070076
- Sibson, R.H. (1991). Loading of faults to failure, *Bull. Seismol. Soc. Am.*, 81, 2493-2497.
- Yamada, M.; J. Mori and T. Heaton (2009). The Slapdown Phase in High-acceleration Records of Large Earthquakes, *Seismological Research Letters* Volume 80, Number 4. doi: 10.1785/gssrl.80.4.559